NUCL SCI TECH (2021) 32:64
https://doi.org/10.1007/s41365-021-00891-1

Radio frequency conditioning of an S-band accelerating structure prototype for compact proton therapy facility

Yu Zhang[1,2,3] · Wen-Cheng Fang[1,4] · Xiao-Xia Huang[4] · Jian-Hao Tan[4] · Shao-Peng Zhong[4] · Cheng-Cheng Xiao[4] · Jun-Qiang Zhang[4] · Cheng Wang[1,2] · Yu-Qing Yang[1,2,3] · Zhen-Tang Zhao[1,2,3,4]

Received: 4 March 2021 / Revised: 15 April 2021 / Accepted: 19 April 2021 / Published online: 17 June 2021

Abstract The development of a high-gradient accelerating structure is underway to construct a compact proton linear accelerator for cancer treatment. Extensive experiments and numerous studies are being conducted to develop compact linear accelerators for proton therapy. Optimization of the electromagnetic and mechanical design has been performed to simplify the manufacturing process and reduce costs. A novel high-gradient structure with a low relativistic proton velocity (β), $v/c = 0.38$, was designed, fabricated, and tested at high power. The first full-scale prototype was also successfully tested with high radio frequency (RF) power, a repetition rate of 50 Hz, and pulse length of 3 μs to reach a high-gradient of 46 MV/m using a 50 MW S-band klystron power supply obtained from the Shanghai Soft X-ray Free Electron Laser Facility. This is the first high-power test in China, which is in line with the expected experimental goal. This study presents preliminary high-power testing of S-band standing wave accelerating structures with 11 cells. This work aims to verify the feasibility of using a high-gradient RF accelerating structure in compact proton therapy facilities. The cold test of the prototype cavity was completed in advance. Details of the high-power RF test setup, the process of RF conditioning, and the high-power results are described.

Keywords S-band · Standing wave (SW) · High-gradient · Accelerating structure · RF conditioning

1 Introduction

Proton therapy, also known as proton beam radiotherapy, is an essential component of particle radiotherapy. Owing to the excellent protection, it provides to normal tissues and its biological effects near the Bragg peak, proton therapy has gained the approval of an increasing number of doctors and is favored by patients [1]. In recent years, many proton therapy centers have been established globally [2, 3]. As of February 2021, there are approximately 111 facilities dedicated to proton or heavy-ion therapy worldwide. Proton therapy is the primary method of heavy-ion therapy, which accounts for approximately 89% of heavy-ion therapy. There are approximately 37 particle therapy facilities under construction, and approximately 26 are planned to be built-in future [1]. According to the current requirements for single-room facilities, ultra-high dose rate (FLASH) radiotherapy [4], and proton computed tomography (CT) [5], research on compact and efficient accelerators for proton therapy equipment has gained considerable attention. In a single-room facility, the linear accelerator (linac) is directly installed on a rotating gantry, which makes the proton therapy facility more compact and cost efficient. In clinical practice, the

This work was supported by National Key R&D Program of China (No. 2018YFF0109203).

✉ Wen-Cheng Fang
fangwencheng@zjlab.org.cn

✉ Xiao-Xia Huang
huangxiaoxia@sinap.ac.cn

[1] Shanghai Institute of Applied Physics, Chinese Academy of Sciences, Shanghai 201800, China

[2] University of Chinese Academy of Sciences, Beijing 100049, China

[3] ShanghaiTech University, Shanghai 201210, China

[4] Shanghai Advanced Research Institute, Chinese Academy of Sciences, Shanghai 201204, China

accuracy of proton therapy is essential to the quality of treatment [6, 7]. The accuracy can be improved using proton CT, which solves the error of conversion from traditional CT to proton therapy. The minimum beam energy required for the beam to pass through the human body is 350 MeV. A section of the booster can be connected to the existing proton therapy facility, and the high-gradient linac can be used to achieve an energy upgrade. FLASH therapy requires ultra-high dose irradiation in a short time. A single short pulse (< 100 ms) is delivered at an ultra-high dose rate that exceeds 100 Gy/s [8], which significantly exceeds the conventional dose rate of 0.05 Gy/s; only a linac can achieve such rapid energy modulation. The most representative devices at present are IMPULSE [9], TULIP [10], and ProBe [11]. Further research will make proton therapy facilities more popular and preferential, which will significantly promote proton therapy development.

The current development of high-gradient radio frequency (RF) technology can contribute to achieving a more compact and efficient proton therapy device. Compared with synchrotron radiation accelerators and cyclotrons, linacs can easily meet the requirements of compact proton therapy facilities. In the early 1990s, Hamm et al. first proposed the use of an S-band linac for proton therapy [12, 13]. The TERA Foundation proposed and designed a proton therapy facility based on a high-frequency linac [14, 15] and developed a scheme based on a high-gradient linac, which combines a cyclotron used as an injector with a high-gradient linac used as a booster [16, 17]. The main component of the entire accelerator facility is the linear accelerating structure with a high accelerating gradient, which can be used to make the linac more compact and cheaper [18].

Research and development of high-gradient RF technology is essential to develop proton therapy technology. The Shanghai Advanced Proton Therapy Device (APTRON) is the first hospital-based proton therapy facility in China [19, 20]; however, its design is based on a synchrotron radiation accelerator. We conducted a series of investigations and designed an all-linac proton accelerator based on a high-gradient linear accelerating structure [21]. The energy of the S-band proton therapy linac that we designed is adjustable from 70 to 250 MeV; the average current intensity is 20 nA, and the pulse width is 10 μs with a repetition frequency of 1000 Hz. The linac consists of an ion source, the radio frequency quadrupole (RFQ), the side-coupled drift Tube Linac (SCDTL), the main accelerating structure (2856 MHz), permanent magnet quadrupoles (PMQs), and a power source. The overall length of the accelerator is less than 7 m. The designed all-linac proton therapy facility scheme is shown in Fig. 1. For the design of the main accelerating structure, we chose a relatively high operating frequency (up to the S-band) to reduce the cavity size. However, the higher the operating frequency, the smaller is the radial size of the accelerating cavity, and the greater is the manufacturing difficulty. For this, we chose a standing wave (SW) accelerating structure with an operating frequency in the S-band. In addition to considering the breakdown field strength when selecting the accelerating electric field gradient, the cavity consumption must be considered for the design of the accelerating structure, which is applied to a proton linac with a relatively large duty cycle. This accelerator is characterized by its compact structure and low cost. The proton energy must also be adjusted by turning off a part of the high-frequency power source or changing the input power. The linac uses a series of PMQs to focus the beam size and reduce the emittance growth; the PMQs are also used to reduce the overall size and the subsequent operation energy consumption.

The development of the main accelerating structure of the linac is complete, and the optimization of the accelerating structure, processing and manufacturing, low-power testing, and tuning is complete as well and is described in detail in Ref. [21]. Compared with the backward traveling wave (BTW) structure, we adopt a SW accelerating structure; the operating model of the BTW structure is a $5\pi/6$ mode, while that of the accelerating structure introduced in this study is a π mode, which has a high shunt impedance. For low-beta accelerating structures, it is difficult to control the traveling wave phase and synchronize the proton beam with the electromagnetic field. This study describes a high-power test of a high-gradient accelerating structure. A high-power test was conducted on the Shanghai Soft X-ray Free Electron Laser Facility (SXFEL) facility platform. The high-gradient experiment on the accelerating structure is essential in the development of compact proton therapy equipment. The purpose of high-power testing is to verify the performance of all aspects of the accelerating structure.

After a series of processing, the high-gradient accelerating structure retains a large amount of residual adsorbed gas inside the accelerating structure. There are also some raised particles on the surface of the cavity, which will become a field emission source and affect the performance of the accelerating structure. Therefore, before the high-gradient accelerating structure is applied to the actual project, it needs to go through high-power testing to reduce the particle emission sources in the RF cavity. This enables the high-gradient accelerating structure to operate at a higher electric field. The purpose of RF conditioning is to enable the particle accelerating cavity to operate stably at a high input power, and it does not produce RF discharge in the required vacuum range. RF conditioning has four main functions [22, 23]:

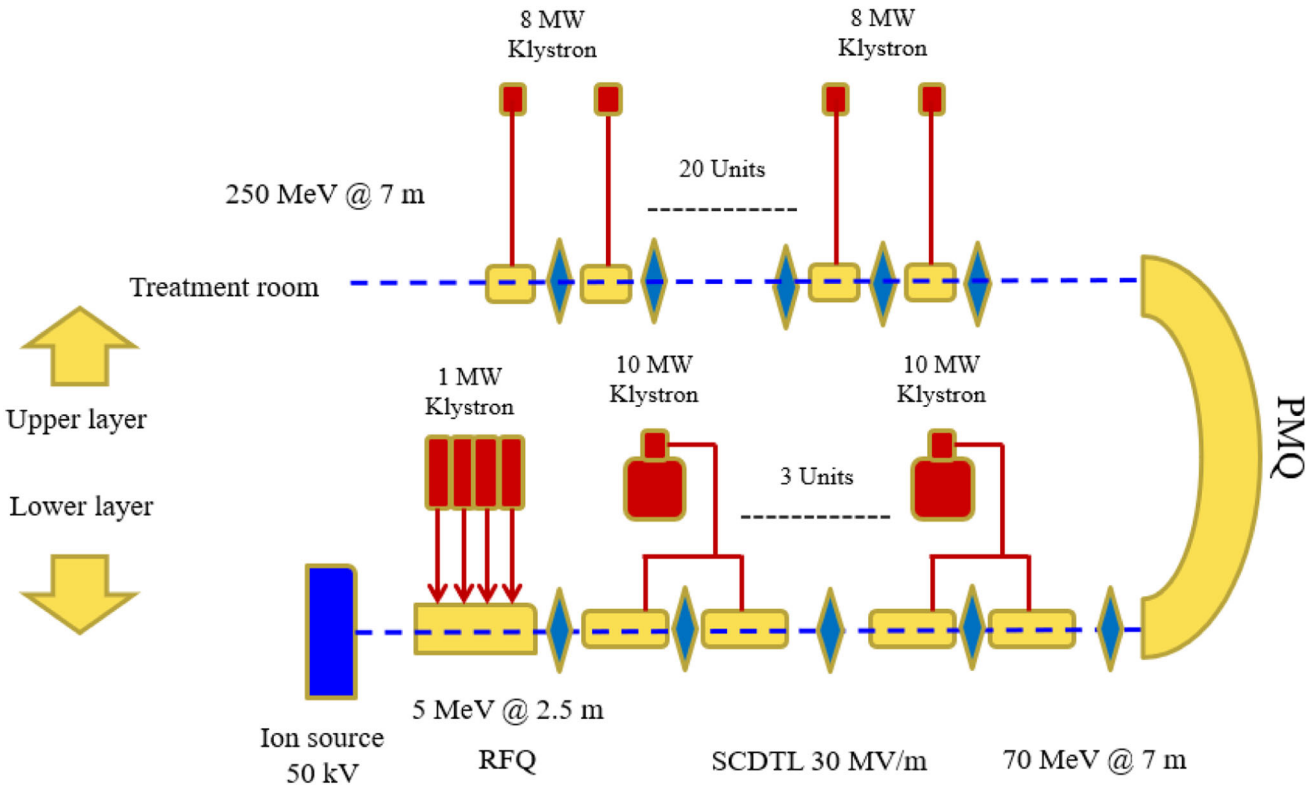

Fig. 1 (Color online) Layout of all-linac scheme

(1) Remove the remaining adsorbed gas in the accelerating cavity.
(2) Remove the dielectric impurities on the internal surface of the accelerating cavity.
(3) Burn whiskers or micro-protrusions on the inner surface of the accelerating cavity and smoothen the surface roughness, pits, and mountains.
(4) Detect the location and frequency of "breakdowns" as well as analyse and find possible processing defects.

In this study, we will primarily introduce the high-power test of the S-band SW accelerating structure conducted on the SXFEL facility platform. We present the design and installation of the high-power RF conditioning platform and the results and analysis of RF conditioning.

2 High-power test platform

The designed accelerating structure is a single periodic S-band SW structure. The accelerating structure consists of π-mode standing wave (SW) cavities and a circular waveguide fed with the TM_{01} mode because the disk-loaded waveguide cavity of the π-mode operating frequency has the highest shunt impedance among all operating modes. However, it was previously observed in a cold test that the single periodic accelerating structure with a π-mode operating frequency is unstable [21]. This instability indicates that the mode interval between adjacent operating frequencies is too small, and the mode jumps are likely to occur during the actual operation of the accelerating structure. Furthermore, the field distribution will experience interference from adjacent modes.

This can be theoretically analyzed. In the SW accelerating structure, when the structure resonates in the π-mode, the forward and backward spatial harmonics merge. The amplitude of the composite field then reaches twice the amplitude of a single harmonic, which greatly increases the shunt impedance of the structure. According to resonant circuit theory, the dispersion relation of a single periodic SW accelerating structure can be obtained as follows:

$$\omega_q = \frac{\omega_0}{\sqrt{1 + k_0 \cos\frac{\pi q}{N}}}, \tag{1}$$

where k_0 is the coupling coefficient between the accelerating structures, ω_0 is the resonant frequency of the accelerating structure, and $\frac{\pi q}{N}$ is the average phase shift between two adjacent accelerating structures. According to the dispersion relation, the frequency difference between the π-mode and its adjacent modes is

$$\left.\frac{\Delta\omega}{\omega_0}\right|_{\pi} = \frac{k_0\pi^2}{4N^2}. \tag{2}$$

This is the narrowest mode interval. From the above analysis, it can be concluded that when the selected operating mode of the accelerating structure is the π-mode, it has a higher shunt impedance, but is less stable [24].

Although the accelerating structure is unstable, we completed the low-power test and subsequent high-power test after careful calculation, simulation, and manufacturing. The experimental results are consistent with the design goal. Although the reflected power is large, the circulator can ensure that the reflected power will not return to the klystron; thereby preventing damage to the klystron. This verifies the feasibility of this accelerating structure; however, owing to its instability, it cannot be used in practical projects. We subsequently developed a biperiodic SW accelerating structure with an operating mode of $\pi/2$, which included the design of the accelerating structure and the optimization of physical quantities. The specific content is not included here. It is used to study the accelerating structure of the linac of a compact proton therapy facility. A low-β single periodic accelerating structure with an expected accelerating gradient of 50 MV/m was designed. The prototype, fabrication, low-power test, and tuning was completed for this design in 2020. The low-power test results after tuning at room temperature (25.8 °C) and standard atmospheric pressure are as follows: the operating frequency of the accelerating structure is 2852.88 MHz, the S parameter at this frequency is − 6.57 dB, and the standing wave rate (SWR) is 2.78. The accelerating structure is in a state of under-coupling, as shown in the Smith chart of the previous microwave measurement in Fig. 2. Although the SWR is relatively large (higher power reflection), there is a circulator between the accelerating structure and the klystron during the high-power test, and the reflected power will not cause damage to the klystron. The final measurement results show that the S-band SW accelerating structure is suitable for high-power testing.

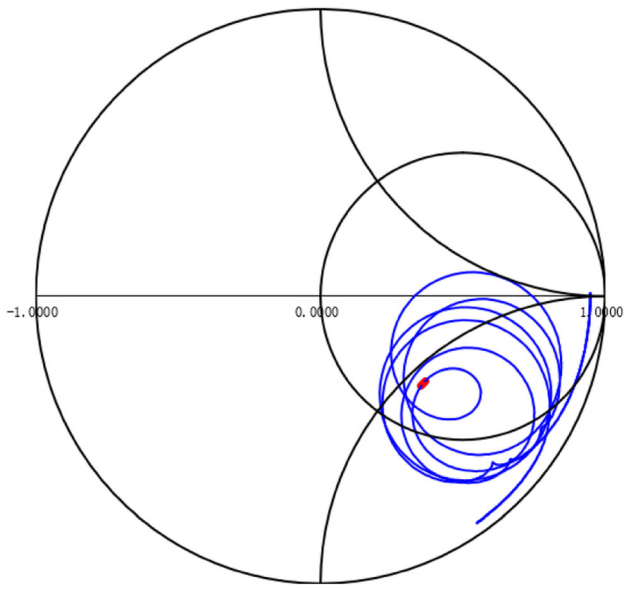

Fig. 2 (Color online) Smith chart

The accelerating structure is part of our research on a high-performance proton therapy facility, which is a single-room proton therapy facility with the unique feature of a linac mounted on a rotating gantry [14]. From this perspective, the high-gradient structure significantly improves the compactness and lightness of the rotating mechanism, while also benefitting the cost and reliability [25]. The high-power test was completed in January 2021. The following describes the layout and feasibility of the high-power testing.

The first prototype structure was subject to a high-power test using an S-band 50 MW klystron power supply from the SXFEL. According to our calculations, if the accelerating gradient of the accelerating structure is 50 MV/m, the power input to the accelerating structure is approximately 9.15 MW. The formula is as follows:

$$\mathrm{ZTT} = \frac{E_0^2 T^2}{P_1} = \frac{\left[\int E(z)\mathrm{d}z\right]^2 T^2}{P}\frac{1}{l}, \tag{3}$$

where ZTT is the effective shunt impedance, $\mathrm{ZTT} = 59.983\ \mathrm{M\Omega/m}$, P_1 is the power loss per unit length, T is the transit time factor of the accelerating structure, $T = 0.846$, and E_0T is the accelerating gradient design value of the accelerating structure, $E_0T = 50\ \mathrm{MV/m}$.

On the SXFEL platform, the machine time is limited because there are other accelerating tubes that require high-power testing. Considering the power transmission attenuation, a quarter of the power of the 50 MW klystron (approximately 12.5 MW) can be distributed to the accelerating structure through a 6 dB power divider, which can meet the requirement of the accelerating structure for high-power testing. The remaining power of the klystron (37.5 MW) is allocated to another accelerating structure. Moreover, high-power testing of the proton accelerator tube is installed on the SXFEL platform using SXFEL's existing technical conditions and equipment and the waveguide system. The original facility uses a 6 dB power divider; and this high-power test did not damage the original facility. After the high-power testing is complete, the normal operation of the SXFEL must be restored. More details on the SXFEL facility can be found in Ref. [26]. The layout of the test platform of the SXFEL facility is shown in Fig. 3; 1 indicates a klystron, 2 is a laser device, 3 is an electron gun, and 4 is an accelerating structure. The accelerating structure is installed in the position of the electron gun. During the installation procedure, nitrogen gas flow, from the inside to the outside of the system, prevented any contamination from dust [14]. Next, we

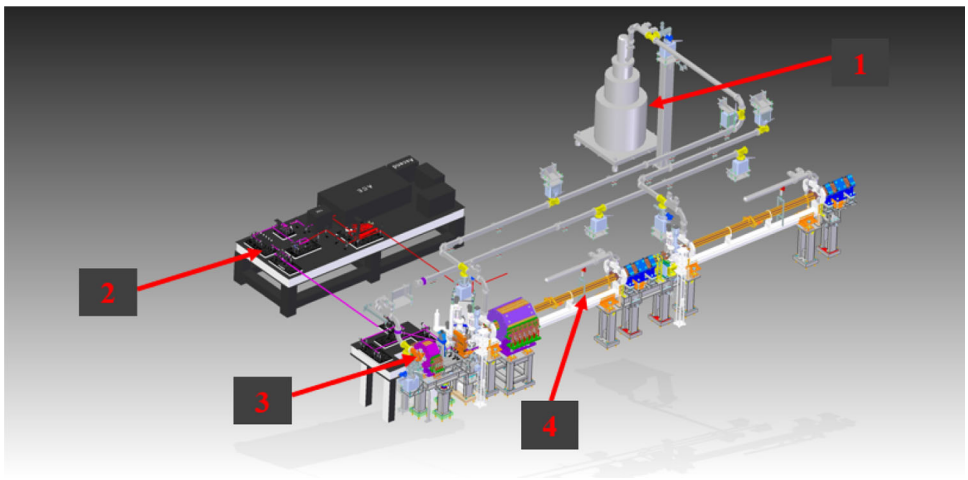

Fig. 3 (Color online) Layout of the test platform of the SXFEL facility

introduce the process of installing this accelerating structure in the SXFEL facility in detail.

The installation of the S-band accelerating structure began on December 3, 2020. To ensure the vacuum degree of the entire system, each component was individually installed and vacuumed, and leak checks were performed during the installation process. Gaskets are required to seal the splicing between the waveguide and accelerating structure; however, the entire device still leaked during the initial installation process. This occurred because the gaskets were not annealed, and the annealed gaskets were fitted at a later time. The installation process proceeded smoothly and required approximately 2 weeks.

Before being installed on the high-power test platform, the accelerating structure's RF parameters must be measured for the klystron's parameter setting. The RF parameters were measured in the SXFEL tunnel. The device diagram for RF parameter measurement is shown in Fig. 4.

The molecular pump is used for vacuuming, and the vacuum degree is 5.49×10^{-7} mbar. A network analyzer is used for the RF measurement. The designed accelerating structure adopts a cooling method of four-in and four-out water circulation with built-in water pipes, which is a traditional internal water-cooling method. We installed an adjustable water tank in the SXFEL tunnel to control the temperature of the accelerating structure. The operating frequency of the accelerating structure refers to the frequency in a vacuum environment and at a constant temperature. Changes in temperature, relative humidity, and air pressure are considered for the microwave measurement, and the frequency needs to be corrected. Frequency correction primarily includes two quantities: pressure and temperature [24, 27]. Equation (4) describes the pressure correction:

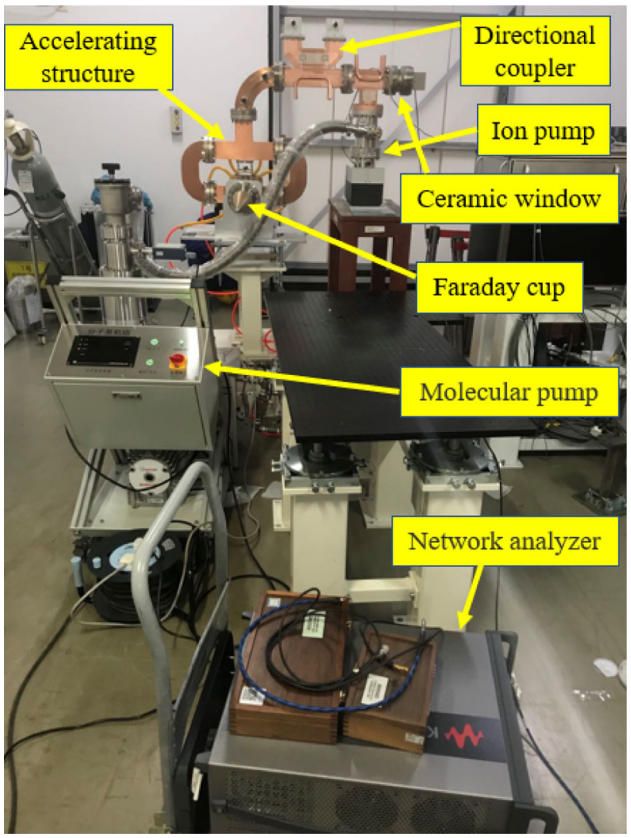

Fig. 4 (Color online) RF parameter measurement device diagram of the prototype cavity

$$
\begin{aligned}
f_{\mathrm{p}} &= \frac{f_0}{\sqrt{\varepsilon_{\mathrm{p}}}}, \\
\varepsilon_{\mathrm{p}} &= 1 + 210 \cdot 10^{-6} \frac{P_{\mathrm{d}}}{T} + 180 \cdot 10^{-6} \left(1 + \frac{3580}{T}\right) \frac{P_{\mathrm{w}}}{T}, \\
\Delta f_{\mathrm{p}} &= f_{\mathrm{p}} - f_0 = f_0 \left(\frac{1}{\sqrt{\varepsilon_{\mathrm{p}}}} - 1\right),
\end{aligned}
\tag{4}
$$

where Δf_p represents the change in pressure with respect to frequency, P_d is the pressure of dry gas, P_w is the pressure of water vapor, and T is the absolute temperature. Assuming $f_0 = 2856$ MHz, $P_d = 760$ Torr, $T = 298.95$ K, a humidity of 77%, and $P_w = 17.54$ Torr, then $\Delta f_p = -0.958$ MHz.

Changes in the cooling water temperature and cavity working temperature may change the temperature of the accelerating structure. Equation (5) describes the temperature correction:

$$\frac{df}{dT} = -gf_0. \tag{5}$$

The influence of temperature on the frequency is related to the sensitivity of the structure size. The accelerating structure is made of copper, and g is the corresponding expansion coefficient, $g = 1.77 \times 10^{-5}/°C$. In the formula, Δf_T represents the change in temperature with respect to frequency. The measuring temperature is 298.95 K, and the working temperature is 293.15 K; thus, $\Delta f_T = f_T - f_0 = -0.293$ MHz [24, 27]. The frequency is increased by 1.251 MHz, and the corrected frequency is (2852.88 − (− 0.958) − (− 0.293))
MHz = 2854.131 MHz.

Considering the change in the working environment of the accelerating structure, the working temperature can be changed by adjusting the temperature of the water tank. Changes in the working temperature of the accelerating structure will result in changes in the accelerating structure operating frequency. We measured the operating frequency of the accelerating structure at different working temperatures. We constructed the temperature-frequency curve from the experiment and compared it with the theoretical value, as shown in Fire 5. The theoretical value is consistent with the measured value. It can be observed from Fig. 5 that the operating frequency of the accelerating structure can be increased by reducing the temperature of the cooling water. However, to achieve the ideal operating frequency, the temperature of the cooling water needs to be reduced below 0 °C, which will freeze the cooling water.

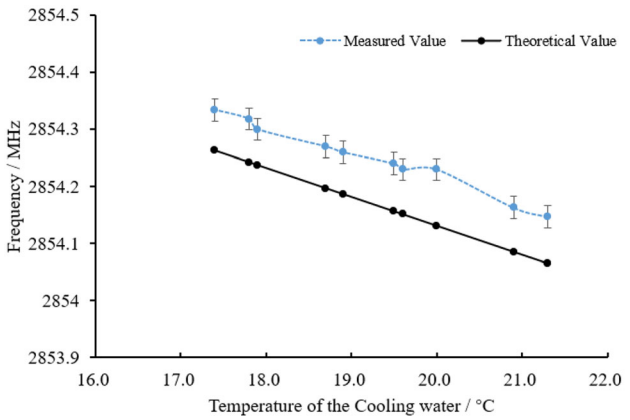

Fig. 5 Temperature-frequency curve of the experiment

After the installation in the SXFEL tunnel, we adjusted the temperature of the cooling water to a suitable temperature of 20 °C. The measured operating frequency was 2854.23 MHz; the difference of 100 kHz from the theoretical value may be owing to other errors, which is consistent with the law. The measured input reflection coefficient at this operating frequency is − 6.2 dB; therefore, the SW ratio is too large, which is an irreparable error caused during processing. This causes the reflected power to increase, and the considerable reflected power may damage the klystron. To solve this problem, two solutions are proposed: the operating frequency of the accelerating structure may be increased by reducing the temperature of the cooling water, alternatively, the klystron frequency can be changed so that it is consistent with the operating frequency of the accelerating structure. Therefore, the reflection is reduced to a level that does not damage the klystron. Considering that the prototype is only used to research RF technology and high-power performance, it can be used for beam testing under the correct conditions. Finally, we adopt a compromised solution by changing the frequency of the klystron to 2854.23 MHz. This is consistent with the operating frequency of the accelerating structure, which can reduce the reflection in the system. The large reflection coefficient may cause excessive power reflection. In the high-power test installation, a 4-port ferrite phase shifter circulator is installed in front of the accelerating structure to recover the reflected power, which can prevent damage to the klystron. The circulator is produced by AFT Microwave (Backnang, Germany). For further details, please refer to the installation diagram of the high-power test platform in Fig. 6b.

The on-site installation diagram of the S-band accelerating structure after the preliminary installation on the high-power test platform is shown in Fig. 6a. The scheme of the S-band accelerating structure high-power test layout is shown in Fig. 6b. In this figure, the ion pump is used to ensure that the vacuum of the entire system meets the experimental standards, and the Faraday cup is used to monitor the dark current. A power divider is installed behind the klystron to distribute a quarter of the power source to the accelerating structure, and the remaining power is distributed to other test equipment. The 4-port circulator behind the ceramic window is used to recover the reflected power and protect the klystron from breakdown due to excessive reflected power. We use two directional couplers, DC1 and DC2, to measure the input waves and the reflected and transmitted waves. The directional couplers were calibrated in the laboratory using waveguide-coaxial transitions and a network analyzer. The power

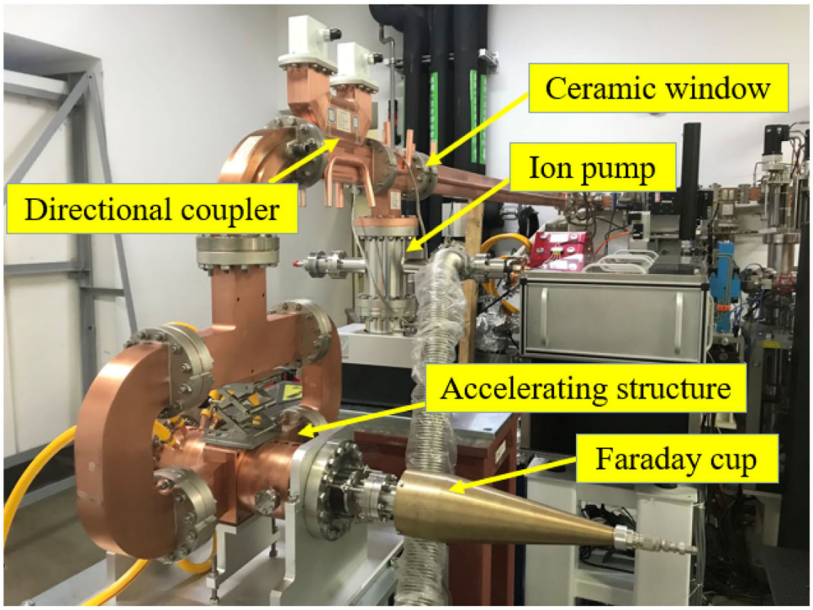

(a)

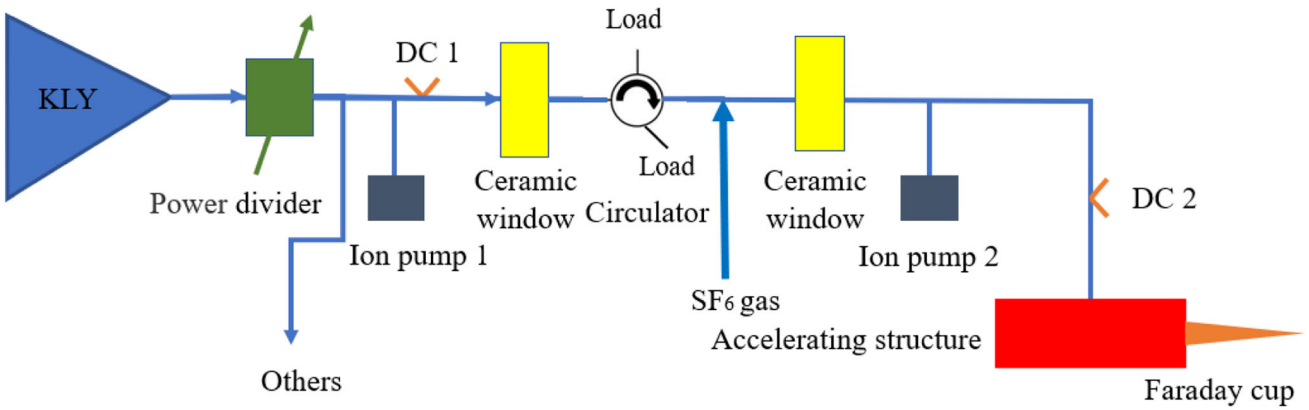

(b)

Fig. 6 (Color online) Site installation diagram and schematic diagram of the S-band accelerating structure on the high-power test platform. **a** On-site installation diagram of the S-band accelerating structure on the high-power test platform. **b** Schematic of the S-band accelerating structure high-power test layout

transmission direction is from port 1 to port 2 of the directional coupler. Port 1 is upstream and is close to the direction of the klystron; port 2 is downstream and is close to the direction of the accelerator tube. Ports 4 and 1 are on the same side, as are ports 3 and 2. The transmission waveguide coefficient S11 of the directional coupler is − 25.91 dB at the operating frequency, S31 and S41 are − 50.40 dB and − 76.76 dB, respectively, and the isolation is approximately − 26.27 dB, which meets the measurement isolation requirements of the directional coupler. Moreover, a ceramic window is inserted to avoid exposing the klystron window to the cavity vacuum during installation and then to under conditioning. The purpose of passing sulfur hexafluoride (SF_6) gas is to ensure the working requirements of the circulator because it cannot operate in a vacuum. On the last day of 2020, we conducted a series of inspections and adjustments for the entire experimental device. The high-power test officially started on January 5, 2021 and ended on January 15, 2021. The entire conditioning procedure is semi-automatic. Next, we introduce the entire conditioning process in detail.

3 Preparation for RF conditioning

The power source is an RF unit based on a solid-state modulator, and a 50 MW S-band high-power pulse klystron (E3730A, Toshiba, Tokyo, Japan) was used for the RF conditioning. The klystron facility is shown in Fig. 7a, and it is located in the technology corridor. After passing the 6 dB power divider, the power allocated from the klystron is approximately 12 MW. We measured the input power at the entrance of the accelerating structure with a power meter and calculated the power attenuation of the fixed attenuator, directional coupler, and cable. The input power of the accelerating structure was calculated to be approximately 9.9 MW. A detailed calculation process is presented in Sect. 2. This result exceeds our experimental goal. The purpose of RF conditioning is to achieve the nominal parameters in terms of the input power at the input coupler (9.15 MW, corresponding to an accelerating gradient of 50 MV/m), the repetition rate (50 Hz), and pulse length (3 μs, corresponding to one filling time).

The relevant measurement personnel of the SXFEL calibrated the power measurement values. The following section briefly introduces the performance of the klystron. The input and output characteristic curves of the klystron are shown in Fig. 7b. The maximum value of the charging voltage of the modulator should not exceed 45 kV. All the data in this figure were measured by the relevant technical personnel of the SXFEL. The charging voltage value of the modulator is manually changed, and the output pulse and output voltage values of the klystron are recorded on the control panel. Figure 7b is a critical reference basis for RF conditioning. In the RF conditioning control interface in the central control room, the charging voltage of the modulator can be changed to complete the high-power test. The output power data of the klystron can be obtained according to the input and output characteristic curve of the klystron. Finally, the accelerating gradient is calculated by calculating the power that is input to the accelerating structure after attenuation. The charge voltage of the modulator gradually increases during the conditioning process; therefore, the power that is input to the accelerating structure increases, and the accelerating gradient also increases accordingly.

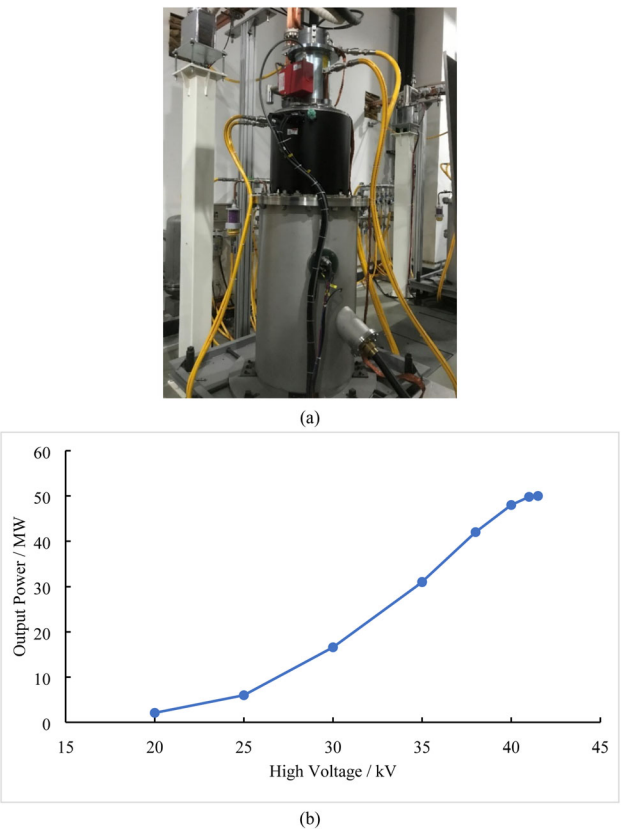

Fig. 7 (Color online) **a** 50 MW S-band high-power pulse klystron. **b** Input and output characteristic curves of the klystron

The input signal, reflected signal, and pickup signal of the RF pulse are shown in Fig. 8. In Fig. 8, the red and blue lines indicate the voltage and RF power, respectively. In the graph of the reflected signal, the blue line is lower than the red line, which indicates that the accelerating structure is under-coupled. If the accelerating structure is in a critically coupled state, the red and blue lines would coincide, and if the accelerating structure is in an over-coupled state, the blue line would be higher than the red line. It can be observed from the shape of the reflected signal that this accelerating structure is under-coupled. This result is consistent with our previous microwave measurement results in Ref. [21].

4 Process and results of RF conditioning

The entire conditioning procedure is semi-automatic, and the modulator charge voltage may be switched off (which is what we often call the breakdown phenomenon) by an artificial breakdown made by local operators or a broken ion pump vacuum, which causes the pressure to exceed the threshold corresponding to 1×10^{-8} mbar or causes the monitored reflection signal of the klystron to be more than twice the normal value. In our conditioning procedure, after a breakdown phenomenon occurs, the conditioning procedure will activate the automatic protection mechanism, whether the phenomenon is due to a vacuum drop, caused by breakdown, or the sparking phenomenon, caused by exceeding the reflected power threshold. First, the modulator's high voltage is automatically decreased by 2 kV, the corresponding input power will decrease, and the high voltage of the modulator is slowly increased by 0.01 kV every 4 s on average. This

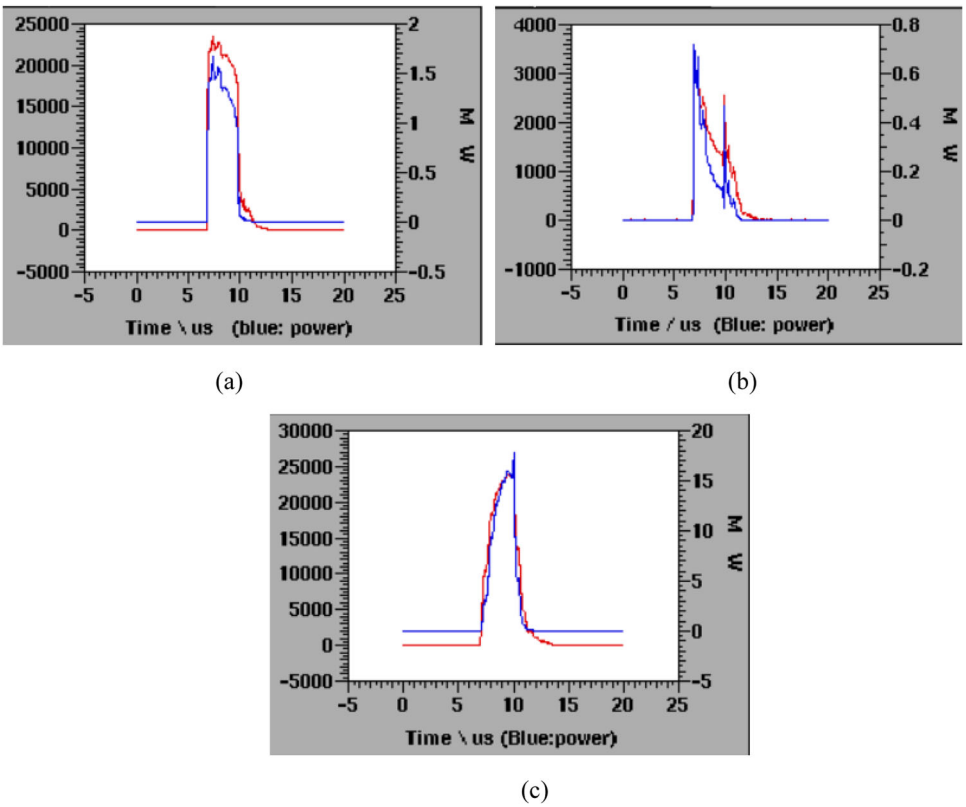

(a) (b)

(c)

Fig. 8 (Color online) The shapes of different RF pulses for **a** the input signal, **b** the reflected signal, and **c** the pickup signal from the cavity. The red and blue lines indicate the voltage and RF power, respectively

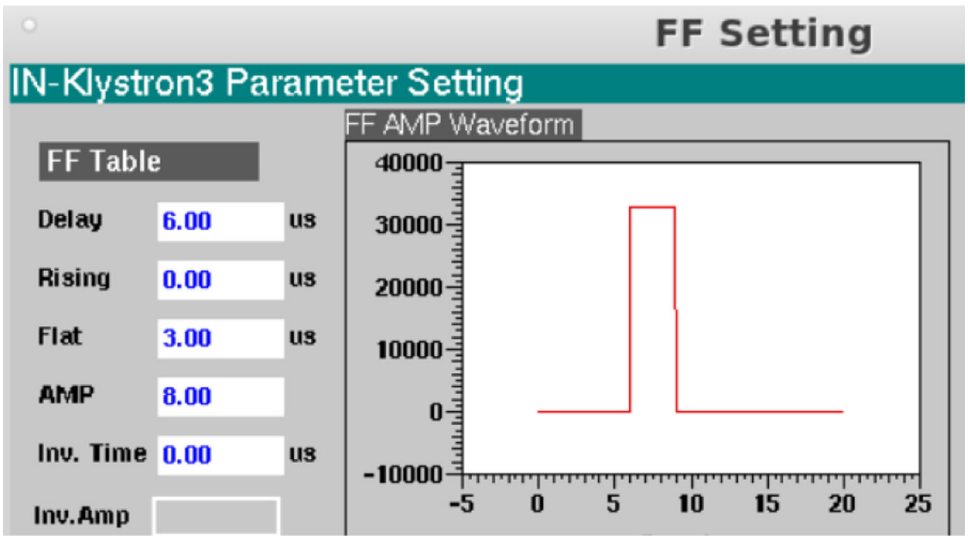

Fig. 9 (Color online) Pulse length

process lasts for several minutes. After 30 s of stable operation under the current input power, the RF high voltage is increased by 0.01 kV. The entire RF conditioning process lasts for approximately 240 h.

We initially set the repetition frequency to 50 Hz and the RF pulse length to 2.5 μs during conditioning. Subsequently, the charging voltage of the modulator is gradually increased. After approximately 200 h, the charging voltage of the modulator rises to 40 kV. Before increasing the RF pulse length, we ran the system stably for 10 h with the maximum charge voltage of the modulator, and no breakdown event occurred. After increasing the pulse length to 3 μs (as shown in Fig. 9), the charging voltage of the modulator increases to 40 kV after a short time.

The high-voltage signal of the modulator is recorded, and the high-voltage trend during the entire high-power experiment is shown in Fig. 10. As can be observed in the figure, in the early stage of the high-power testing, the

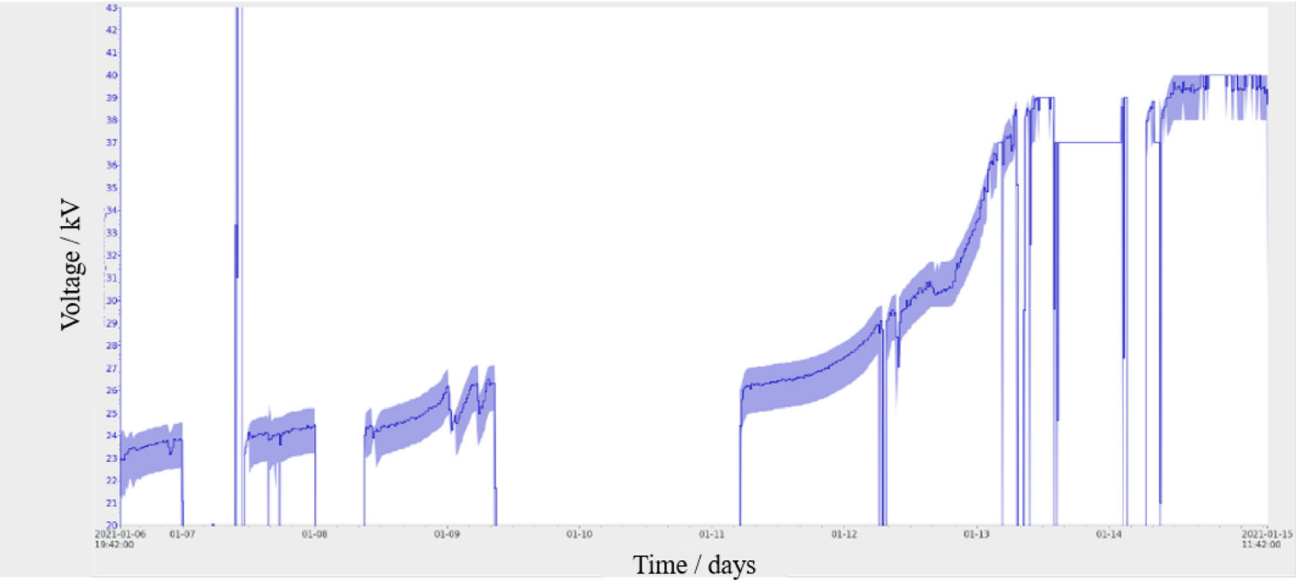

Fig. 10 Trend of modulator high voltage change

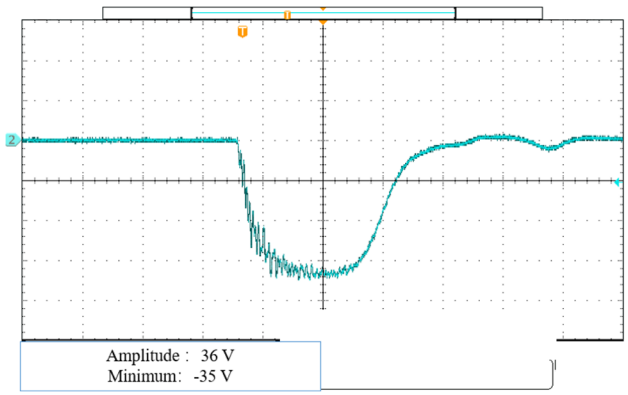

Fig. 11 Pulse current of the klystron measured by the oscilloscope

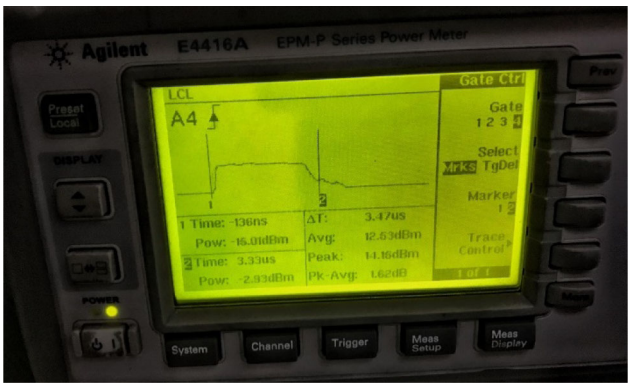

Fig. 12 (Color online) Snapshot of the actual input power value of the accelerator tube measured by the power meter

Table 1 Attenuation of each component

Components	Decrement (dB)
Cable	7.41
Directional coupler	50.40
Fixed attenuator	28

modulator's high voltage rises slowly, and breakdowns are frequent. This occurs because the proton-accelerating structure has recently left the factory, which indicates that there may be more burrs or residual gas inside the cavity. The intermediate interruption is owing to the installation of other equipment by the SXFEL equipment, and not because the equipment is malfunctioning. The high voltage rise of the modulator in the later stage is faster because the cavity inner surface burr decreases, and the internal residual gas is reduced after the previous RF conditioning; this improves the working environment in the cavity. Therefore, the number of breakdowns in this stage is reduced. Finally, the system runs stably while maintaining a very low breakdown rate.

The pulse current of the klystron measured by the oscilloscope is shown in Fig. 11. In this figure, we can observe that the measured minimum value is − 35 V, and the klystron pulse current is calculated to be 350 A. The output pulse current value of the klystron is verified. This value is obtained based on the current transformer monitor with a nominal ratio of 10:1; the related theory can be found in Ref. [28].

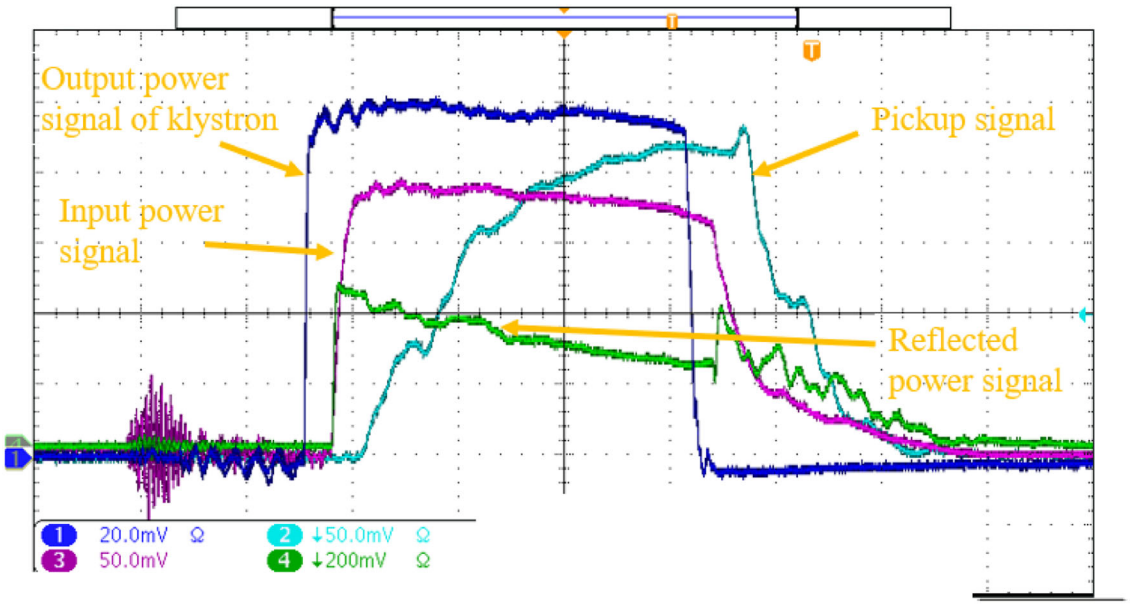

(a)

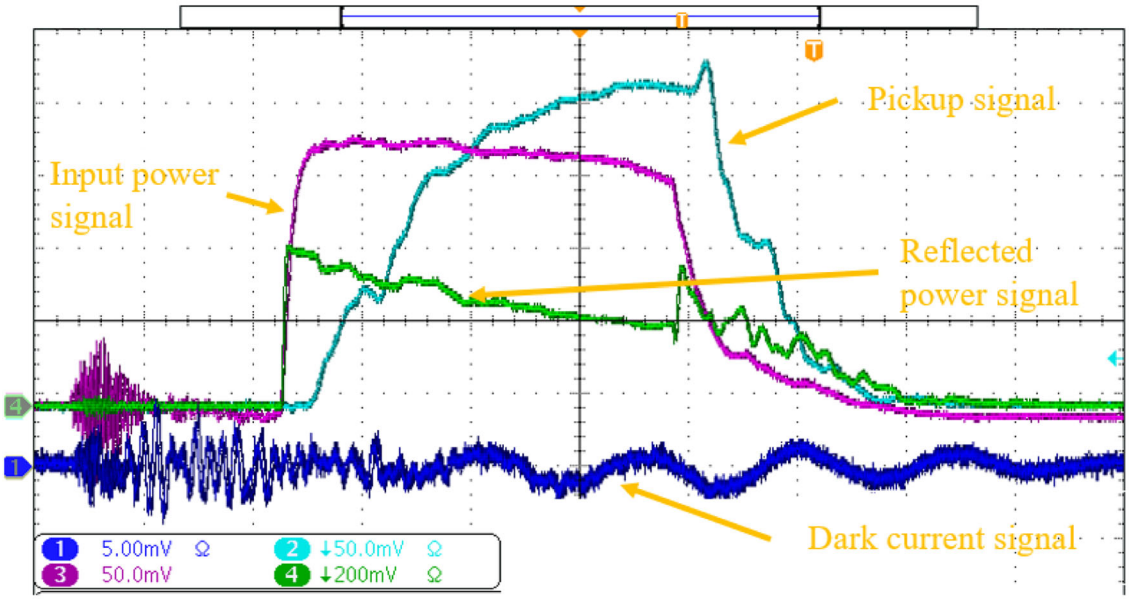

(b)

Fig. 13 (Color online) Four signals collected by an oscilloscope in the case of an approximate input power of 9.9 MW and pulse length of 3 μs pulse length. **a** Input and reflected power signals of the accelerating structure, output power signal of the klystron, and pickup signal. **b** Input and reflected power signals of the accelerating structure, dark current signal, and pickup signal

We use a power meter to measure the input power at the entrance of the proton-accelerating structure. The measurement result is shown in Fig. 12, and the value is 14.15 dBm. The attenuations of the directional coupling cavity, fixed attenuator, and cable are shown in Table 1. The input power at the entrance of the proton-accelerating structure is P_{in}. From the formula $10\log_{10} P_{\text{in}}(\text{mW}) = \hat{P}(\text{dBm})$, P_{in} can be calculated to be 9.9 MW. From this value, the input power at

Table 2 Design and measurement values of S-band standing wave accelerating structure

	Design values	Measurement values
Frequency, f (MHz)	2856	2854.23
Operating mode	π	π
Cell Length, L (mm)	19.958	19.958
Shunt impedance (MΩ/m)	83.816	
Transit time factor	0.846	
ZTT (MΩ/m)	59.983	
Cell no	11	11
SWR	1	2.78
Accelerating gradient $E_a = E_0 \times T$ factor (MV/m)	50	46
Input power (MW)	9.15	9.9
Filling time (μs)	0.256	0.375

the entrance of the proton-accelerating structure is obtained as 9.9 MW.

The incident power at the entrance of the proton-accelerating structure is P_{in}, part of which enters the accelerating structure, P_{cav}; some power is reflected as reverse power, P_{rev}. The incident power is the sum of the cavity and reverse power, $P_{in} = P_{cav} + P_{rev}$. The incident power enters the accelerating cavity through a coupling hole with the waveguide cavity coupling parameter β_c. The reverse power is given by [29]

$$P_{rev} = P_{in}\left(\frac{\beta_c - 1}{\beta_c + 1}\right)^2. \quad (6)$$

The effective input power entering the acceleration cavity can be calculated as $P_{cav} = P_{in} - P_{rev} = 7.7$ MW. According to Eq. (3), the actual accelerating gradient can be calculated to be 46 MV/m.

We increased the input power to a maximum of 9.9 MW, which theoretically means that the accelerating gradient of the S-band accelerating structure has reached the expected goal. However, owing to processing errors, the SWR and reflected power are too large, which eventually causes the accelerating gradient to be slightly different from the theoretical value. This indicates that the proposed high-gradient accelerating structure for a compact proton therapy facility was successfully manufactured, and the measurement was completed. This prototype provides valuable experience for future proton therapy facilities. Details on the process and results of the high-power test will be presented next.

For an input power of approximately 9.9 MW and a pulse length of 3 μs, we use an oscilloscope to measure the input and reflected power signals of the accelerating structure, the output power signal of the klystron and the pickup signal. The four signals are shown in Fig. 13a. It can also be observed from the reflected signal measured in Fig. 13a that the accelerating structure is under-coupled. An oscilloscope was used to measure the dark current on-site; however, it can be observed from Fig. 13b that no dark current signal is detected. This is because the beam aperture of the accelerating structure is too small to observe the dark current.

To date, all the tests have been completed. According to the tested S-band SW accelerating structure results, all the design goals have been achieved. Table 2 lists the design targets and measured values. The measurement result shows that the effective input power is 7.7 MW. According to the above formula (3), the actual accelerating gradient can be calculated as 46 MV/m.

5 Discussion

Initially, an accelerating structure with a single periodic operating frequency in the π-mode was chosen because it corresponded to the highest shunt impedance. However, it was observed that the operation of the single periodic accelerating structure was unstable. If the mode interval is too small, it would cause jumps between adjacent modes. We will subsequently conduct an investigation on the biperiodic SW accelerating structure for proton therapy facilities, including the side-coupled SW accelerating structure and the axis-coupled accelerating structure. The Institute of Nuclear Science and Technology, Sichuan University, China, proposed the construction of a 3 GHz side-coupled cavity linear accelerator (SCL) to reaccelerate the 26 MeV proton beam extracted from the CS-30 cyclotron to 120 MeV [30]. However, the ultimate design goal of the accelerating structure that we designed is to increase the energy of the proton beam to 350 MeV to meet the proton energy required by proton CT.

6 Conclusion

A prototype of the S-band accelerating structure was successfully designed, fabricated, and tuned. Subsequently, the high-power test platform was set up in the tunnel of the SXFEL. After RF conditioning for approximately 240 h, the prototype structure was completed, and a high-power test was performed with an input power of 9.9 MW, under the condition of a 50 Hz repetition rate and 3 μs pulse length. The results of the high-power test mostly verified the design of the S-band high-gradient technology. More importantly, the results demonstrated the strong feasibility of developing compact proton therapy facilities based on the high-gradient linac. The development of an S-band SW accelerating structure prototype provides valuable experience and a solid foundation for the research, development, and construction of critical technologies for future proton therapy facilities.

Author contributions All authors contributed to the study conception and design. Material preparation, data collection, and analysis were performed by Yu Zhang, Wen-Cheng Fang, Xiao-Xia Huang, Jian-Hao Tan, Shao-Peng Zhong, Cheng-Cheng Xiao, Jun-Qiang Zhang, Cheng Wang, Yu-Qing Yang, and Zhen-Tang Zhao. The first draft of the manuscript was written by Yu Zhang and all authors commented on previous versions of the manuscript. All authors read and approved the final manuscript.

References

1. Particle Therapy Cooperative Group (PTCOG) Collaboration. http://www.ptcog.com.
2. P.J. Bryant, L. Badano, M. Benedikt et al., Proton-ion medical machine study (PIMMS). CERN (1999). https://doi.org/10.1007/bf03038873
3. Y.-H. Yang, M.-Z. Zhang, D.-M. Li, Simulation study of slow extraction for the Shanghai Advanced Proton Therapy facility. Nucl. Sci. Tech. **28**, 120 (2017). https://doi.org/10.1007/s41365-017-0273-0
4. A.J. Lennox, Hospital-based proton linear accelerator for particle therapy and radioisotope production. Nucl. Instrum. Methods Phys. B **56–57**, 1197–1200 (1991). https://doi.org/10.1016/0168-583X(91)95130-6
5. R. Cassetta, P. Piersimoni, M. Riboldi et al., Accuracy of low-dose proton CT image registration for pretreatment alignment verification in reference to planning proton CT. J. Appl. Clin. Med. Phys. **20**(4), 83–90 (2019). https://doi.org/10.1002/acm2.12565
6. H.F. Ou, B. Zhang, S.J. Zhao, Gate/Geant4-based Monte Carlo simulation for calculation of dose distribution of 400 MeV/u carbon ion beam and fragments in water. Nucl. Sci. Tech. **27**, 83 (2016). https://doi.org/10.1007/s41365-016-0097-3
7. J. Wang, X. Pei, R.F. Cao et al., A multiphase direct aperture optimization for inverse planning in radiotherapy. Nucl. Sci. Tech. **26**, 010502 (2015). https://doi.org/10.13538/j.1001-8042/nst.26.010502
8. W.-C. Fang, X.-X. Huang, C.-P. Wang et al., Proton linac-based therapy facility for ultra-high dose rate (FLASH) treatment. Nucl. Sci. Tech. **32**, 34 (2021). https://doi.org/10.1007/s41365-021-00872-4
9. C. Ronsivalle, A. Ampollini, G. Bazzano et al., The top implart linac: machine status and experimental activity. Proc. IPAC (2017). https://doi.org/10.18429/JACoW-IPAC2017-THPVA090
10. S. Benedetti, A. Grudiev, A. Latina, High gradient linac for proton therapy. Phys. Rev. Accel. Beams **20**, 040101 (2017). https://doi.org/10.1103/PhysRevAccelBeams.20.040101
11. S. Pitman, R. Apsimon, G. Burt, et al., ProBE: Proton boosting extension for imaging and therapy, in *Proceedings of 28th Linear Accelerator Conference, East Lansing, Michigan, USA 25–30 Sep 2016*. https://doi.org/10.18429/JACoW-LINAC2016-MOPLR066.
12. C.-Q. Yu, Study on design of proton linacs (in Chinese). https://inis.iaea.org/collection/NCLCollectionStore/_Public/33/023/33023243.pdf
13. R.W. Hamm, K.R. Crandall, J.M. Potter, Preliminary design of a dedicated proton therapy linac, in *Conference Record of the 1991 IEEE Particle Accelerator Conference, San Francisco, CA, USA*, vol. 4, pp. 2583–2585 (1991).https://doi.org/10.1109/PAC.1991.165037
14. A. Degiovanni, U. Amaldi, D. Bergesio, et al., Design of a fast-cycling high-gradient rotating linac for proton-therapy, in *Proceedings of International Particle Accelerator Conference - IPAC13, Shanghai, China*, pp. 3642–3644 (2013). https://accelconf.web.cern.ch/IPAC2013/papers/thpwa008.pdf
15. S. Verdú-Andrés, U. Amaldi, A. Faus-Golfe, CABOTO, a high-gradient linac for hadron-therapy. J. Radiat. Res. **54**(Suppl 1), i155–i161 (2013). https://doi.org/10.1093/jrr/rrt053
16. U. Amaldi, P. Berra, K. Crandall *et al.*, LIBO-a linac-booster for proton therapy: Construction and test of a prototype. Nucl. Instrum. Meth. Phys. A 521, 512–529 (2004). https://doi.org/10.1016/j.nima.2003.07.062.
17. C. De. Martinis, D. Giove, U. Amaldi et al., Acceleration tests of a 3 GHz proton linear accelerator (LIBO) for hadron-therapy. Nucl. Instrum. Methods Phys. A **681**, 10–15 (2012). https://doi.org/10.1016/j.nima.2012.04.017
18. A. Degiovanni, R. Bonomi, M. Garlasché et al., High gradient RF test results of S-band and C-band cavities for medical linear accelerators. Nucl. Instrum. Methods Phys. A **890**, 1–7 (2018). https://doi.org/10.1016/j.nima.2018.01.079
19. C.H. Miao, M. Liu, C.X. Yin et al., Precise magnetic field control of the scanning magnets for the APTRON beam delivery system. Nucl. Sci. Tech. **28**, 172 (2017). https://doi.org/10.1007/s41365-017-0324-6
20. J. Wu, H. Du, S. Xue et al., Gantry optimization of the Shanghai Advanced Proton Therapy facility. Nucl. Sci. Tech. **26**, 040201 (2015). https://doi.org/10.13538/j.1001-8042/nst.26.040201
21. Y. Zhang, W.-C. Fang, X.-X. Huang et al., Design, fabrication, and cold test of an S-band high gradient accelerating structure for a compact proton therapy facility. Nucl. Sci. Tech. **32**, 38 (2021). https://doi.org/10.1007/s41365-021-00869-z
22. G.-L. Wang, The research of control and measurement of the high-power testing platform based on high-gradient accelerating structures, Master's Thesis. University of Chinese Academy of Sciences (Shanghai Institute of Applied Physics, Chinese Academy of Sciences), 2015.
23. J. W. Wang, G. A. Loew, Progress report on new RF breakdown studies in an S-band structure at SLAC, in *Proceedings of the 1987 IEEE Particle Accelerator Conference: Accelerator Engineering and Technology*. https://inis.iaea.org/search/searchsinglerecord.aspx?recordsFor=SingleRecord&RN=21007682
24. C.-G. Yao, *Electron Linear Accelerator* (Science Press, Beijing, 1986). **(in Chinese)**
25. S. Benedetti, A. Degiovanni, A. Grudiev et al., RF design of a novel S-band backward travelling wave linac for proton therapy,

in *Proceedings of LINAC2014, Geneva, Switzerland* (2014). https://accelconf.web.cern.ch/LINAC2014/papers/thpp061.pdf
26. Z.-T. Zhao, D. Wang, Q. Gu *et al.*, SXFEL A soft x-ray free electron laser in China. Synchrotron Radiation News 30, 29–33 (2017). https://doi.org/10.1080/08940886.2017.1386997.
27. X.-X. Huang, Study of the X-band high gradient accelerating structure and wakefield effects, Ph.D. Thesis. University of Chinese Academy of Sciences (Shanghai Institute of Applied Physics, Chinese Academy of Sciences), 2017. (in Chinese)
28. S. Tanaka, TOSHIBA Pulse Transformer Oil Tank Assembly. SPECIFICATION FOR VT-61181
29. T. Rao, D. H. Dowell, Chapter 2: Normal Conducting RF injectors.
30. H.-Y. Li, X.-M. Wan, W. Chen et al., Optimization of the S-band side-coupled cavities for proton acceleration. Nucl. Sci. Tech. **31**, 23 (2020). https://doi.org/10.1007/s41365-020-0735-7